Mechanics of Advanced Composite Structures

Journal homepage: https://macs.semnan.ac.ir/

Semnan University

ISSN: 2423-7043

Research Article

Experimental Investigation of Residual Stress Measurement on Cold Roll Bonded Al/Cu Composite by Incremental Hole-Drilling Method

Amirmasoud Rahimijonoush, Mohammad Honarpisheh*, Amir Abdollahi, Mehdi Mohammadimehr

Faculty of Mechanical Engineering, University of Kashan, 8731753153, Tehran, Iran

KEYWORDS

Residual Stress;

Al/Cu Composite;

Cold Roll Bonding;

Incremental Hole-Drilling;

Mechanical Properties.

ABSTRACT

Hole drilling is a semi-destructive procedure used to measure residual stress. This type of stress, caused by mechanical and thermal effects, can significantly impact the lifetime of composite specimens. This paper studies the residual stress measurement on aluminum-copper composite specimens. The experimental procedure involved creating five different composite specimens using a rolling machine, and then using ABAQUS software in FEA analysis to calculate the calibration coefficients. The American standard ASTM E837 was used to determine the residual stress measurement. The specimens are manufactured through the Cold Roll Bonding (CRB) process with a rolling machine. The incremental hole-drilling strain gauge method was used, with the MTS-3000 Restan machine, to measure the residual stresses. The aluminum-copper composite specimens were manufactured in different sequences. The results showed that the ultimate tensile strength of aluminum mono-layer was lower than all composite specimens. On the other hand, the ultimate tensile strength of the copper mono-layer was higher than all samples, except rolled Cu-Cu one. Furthermore, a comparison between two-layer and three-layer composite specimens showed that the two-layer specimen stored more residual stress. In general, copper metal has stored more residual stress than aluminum metal.

1. Introduction

The hole-drilling stress relaxation technique is commonly used to measure residual stress. This involves using a Rosette Strain Gauge to measure the relieved strains at the drilled hole. These measured strains are then used to calculate the residual stresses [1, 2]. Residual stresses play a crucial role in the lifespan of structures, as they can either decrease or enhance durability. Positive residual stress can improve the durability of a structure, while negative residual stress will decrease [3]. The hole-drilling method is often classified as a semi-destructive procedure because its failure is localized and does not influence the whole workpiece. Manufacturing processes, including welding, machining, forging, casting, or rolling, often generate residual stress. The ASTM E837-13a standard expresses the measurement procedure with strain gauge rosettes [4]. There are different methods to measure residual stress in hole drilling such as Digital Image Correlation (DIC) [5–8], Electronic Speckle Pattern Interferometry (ESPI) [9–12], and Strain Gauge [13–15].

Bimetal strips and sheets are commonly used in a range of household appliances, such as

* **Mohammad Honarpisheh**
E-mail address: honarpisheh@kashanu.ac.ir
Tel ++98-31-55913404, Fax ++98-31-55913434

refrigerators, and fire extinguishing systems, in the automotive and aerospace industries. Mechanical resistance, corrosion, thermal expansion, and electromagnetic conductivity are the main advantages of bimetallic strips. TAMONOV and SUMIN [16] presented the effect of residual stress and heat treatment of stainless steel-zirconium by neutron diffraction. Varavallo et al. [17] investigated the microstructure and residual stress results of Inconel 625 alloy and A516-70 carbon steel using X-ray diffraction analysis. Fronczeka et al. [18] used the XRD technique to investigate the residual stress distribution before and after performing three-point bending tests on an explosively welded composite of aluminum and titanium. Kotobi and Honarpisheh [19] used the slitting method to investigate the residual stress through the thickness of the explosive welded bimetal, steel–titanium, sample. Kotobi et al. [20] investigated the effects of laser bending process parameters on the bending angle and maximum tensile residual stresses using a multilayer perceptron (MLP) neural network. Fei et al. [21] used crack compliance and X-ray diffraction methods to calculate the internal residual stress on aluminum and copper. Shi et al. [13] presented the state of residual stresses and the maximum in-plane shear stress of the bonded copper-steel laminates using the hole drill method. Alinaghian et al. [15] studied the impact of tool diameter, step-down, and rotational speed on the residual stress of an Al/Cu bimetal. They used single-point incremental forming (SPIF) and the incremental hole-drilling method for their investigation.

Furthermore, composite materials exhibit superior characteristics compared to monolithic materials. For instance, copper-aluminum composites are lightweight electrical wires because they have a lower density than copper and higher thermal and electrical conductivities than aluminum. These methods for bonding copper and aluminum include explosive bonding, mechanical alloying, and roll bonding [22–24]. The literature review indicates that research on bimetallic copper and aluminum regarding residual stress measurement is limited, with none examining the effects of roll bonding. In this study, copper and aluminum are bonded using different stacking sequences by Cold Roll Bonding (CRB). The CRB process is a solid-state welding method in which bonding occurs through joint plastic deformation of the metals [25].

Previous studies reveal that there has been no research into determining the residual stress of two and three-layer composite samples. This study aims to measure the residual stress of aluminum-copper composite samples. The experimental procedure involves creating five different composite specimens using a rolling machine, and the ABAQUS software is utilized in FEA to calculate the calibration coefficients.

2. Materials and Experimental Procedure

2.1. Materials and Surface Preparation

Commercially pure aluminum (Al1050) and pure copper (C11000) strips were used, and their specifications are provided in Table 1. The strips were cut parallel to the rolling direction, with dimensions of 140 mm in length (L), 40 mm in width (W), and 2 mm in thickness (T). Aluminum and copper strips were annealed at 350 C for 20 minutes and 450 C for 30 minutes, respectively. The dirt of strips including dust particles, moisture, and greases can weaken the form of a strong bonding during the cold roll process. Therefore, aluminum and copper strips were immersed in acetone to remove the surface contamination. Afterward, a brushing machine with a stainless steel circumferential brush made of wires 0.3 mm in diameter was used to scratch both sides of strips for better connection.

Table 1. Chemical composition of pure aluminum and pure copper.

	%Si	%Fe	%Mn	%Ni	%Zn	%Sn
Al	0.04	0.22	0.12	58	0.00	3.91
Cu	28.16	0.06	31.04	77.42	18.14	0.02

2.2. Cold Roll Bonding Process

The sequence for the bonding process is as follows: Al-Al, Cu-Cu, Al-Cu, Al-Cu-Al, and Cu-Al-Cu. Next, four corners of the strips were drilled to link the strips with metallic wires. The composite strips from 6 mm (three layers) and 4 mm (two layers) in thickness became 1±0.1 mm after the rolling process. The rolling process was done parallel to the rolling direction of composite strips, with a 75% reduction for two-layer strips by two paths of rolling and an 83% reduction for three-layer strips by three paths of rolling. The CRB process was carried out using a rolling machine with a diameter of 350 mm, a roller length of 400 mm, and powered by a 100 hp electric motor, as depicted in Fig. 1 at the University of Kashan. The uniaxial tensile test was performed using a Hounsfield-H25KS testing machine on dog-bone specimens Fig. 2 according to the ASTM standard E8/E8M−13a [26] at K. N. Toosi University of Technology. The stress-strain curves of tensile tests are shown in Fig. 3.

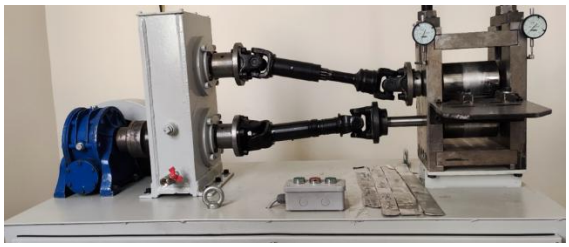

Fig. 1. General view of the rolling machine

Fig. 2. Dog-bone specimens

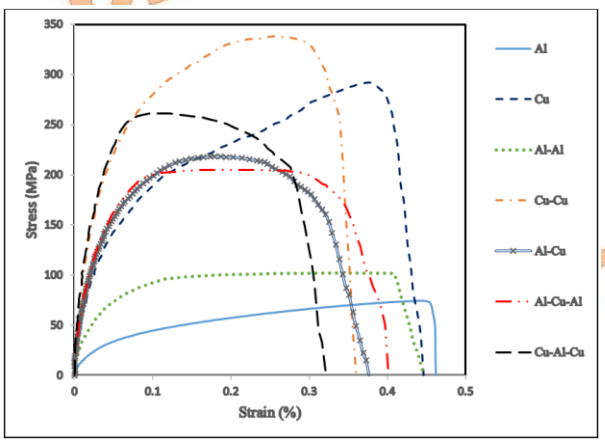

Fig. 3. Engineering stress-strain curves of mono-layer aluminum, mono-layer copper, and annealed composite specimens

2.3. Hole-Drilling Process

The measurement of residual stress was done by the incremental hole-drilling strain gauge method, which is known as the semi-destructive process, on composite specimens comprising Al-Al, Cu-Cu, Al-Cu, Al-Cu-Al, and Cu-Al-Cu shown in Fig. 4. The strain gauge rosette type A, made of MTL-Japan, consists of three strain gauges mounted onto the surface of the composite specimens which are cut into 40 mm (L) and 40 mm (W). The MTS-3000 Restan machine was used to drill incremental holes based on standard ASTM E837, drilling a 2 mm hole as shown in Fig. 4. An inverted cone carbide bur drilling cutter is used as a drill bit for the hole-drilling process.

Then, the residual stress is calculated from the released strains during the hole drilling. The drilling process is performed with steps of 0.05 mm for residual stress measurements. During the drilling, the residual stress was measured by the strain gauge and converted to strains, $\varepsilon_1, \varepsilon_2, \varepsilon_3$, by the data logger.

Fig. 4. MTS-3000 Restan drilling machine

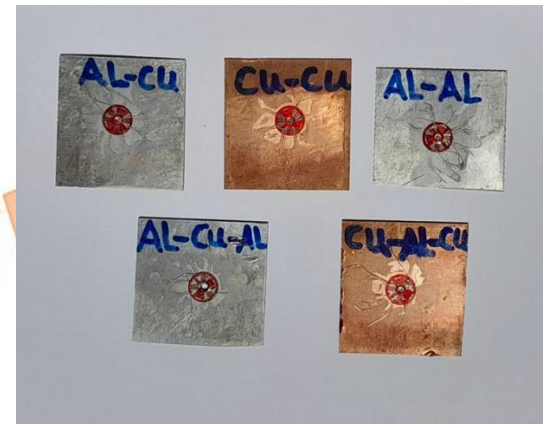

Fig. 5. Hole-drilled composite specimens with attached strain gauge rosette to the surface

3. Results and Discussions

3.1. Uniaxial Tensile Tests

The uniaxial tensile tests were used to obtain the stress-strain curves of mono-layer aluminum, mono-layer copper, and annealed composite specimens represented in Fig. 5 and their ultimate tensile strength in Fig. 6. It shows, that the Cu-Cu specimen has the highest ultimate tensile strength with 337.8 MPa, and the Al specimen has the lowest ultimate tensile strength with 74.5 MPa. Other samples stood in between, Cu with 291.8 MPa, Cu-Al-Cu with 261.3 MPa, Al-Cu with 218.4 MPa, Al-Cu-Al with 205 MPa, and Al-Al with 101.7 MPa. Comparing Al-Al with Al and Cu-Cu with Cu samples, it can be seen that the ultimate tensile strength is increased in double-layer specimens and the elongation is decreased. The existence of copper metal in the arrangement of Cu-Al-Cu specimen shows a higher ultimate

tensile strength rather than Al-Cu-Al, while it is vice versa in elongation.

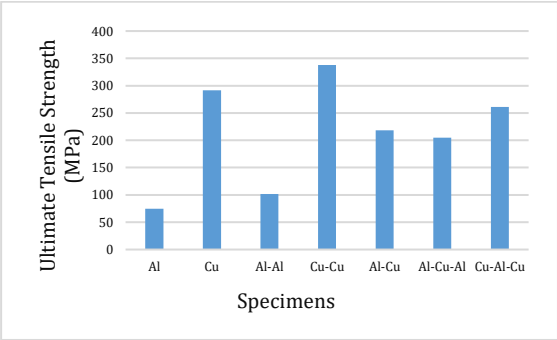

Fig. 6. Ultimate tensile strength of mono-layer aluminum, mono-layer copper, and annealed composite specimens

3.2. Microstructure Observation

The microstructure of the two-layered (Al-Al, Cu-Cu, Al-Cu) and three-layered (Al-Cu-Al, and Cu-Al-Cu) composite specimens produced by CRB are shown in Fig. 7. The optical microscope is used to observe the interlaminar bonding and to obtain the thickness of each layer in composite specimens to calculate the residual stress. The thickness of each layer in the composite specimen consists of Al-Al (0.516 - 0.513) mm, Cu-Cu (0.551 - 0.552) mm, Al-Cu (0.534 - 0.545) mm, Al-Cu-Al (0.389 - 0.342 - 0.372) mm, and Cu-Al-Cu (0.309 - 0.361 - 0.369) mm.

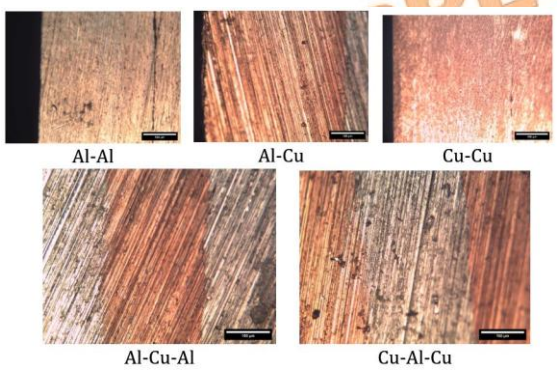

Fig. 7. Microstructure views of the cold roll bonded composite samples

3.3. Residual Stress Measurement

A sheet of the same material and thickness as the original part is modeled to determine the coefficient A_n. The strain gauge is then modeled on the surface of the sheet at its center, allowing for the reading points in directions 1, 2, and 3 to be visible. The sheet is then subjected to biaxial stress with equal values, and the strain values are recorded at predetermined nodes. These values are then substituted into equation 7a to obtain the coefficient A_n at each depth. To determine the coefficients B_n at each depth, the same steps are repeated using equations 6 and 7b. However, instead of introducing tensile stress in the previous step, one direction is subjected to tensile stress and the other direction is subjected to compressive stress, both with equal values.

The strains were measured using a strain gauge rosette, which was attached to the surface of the specimen. The calculation was performed using the following formula:

$$\varepsilon_1 = A(\mathfrak{6}_x + \mathfrak{6}_y) + B(\mathfrak{6}_x - \mathfrak{6}_y)\cos 2\alpha \quad (1)$$

$$\varepsilon_2 = A(\mathfrak{6}_x + \mathfrak{6}_y) + B(\mathfrak{6}_x - \mathfrak{6}_y)\cos 2(\alpha + 45^\circ) \quad (2)$$

$$\varepsilon_3 = A(\mathfrak{6}_x + \mathfrak{6}_y) + B(\mathfrak{6}_x - \mathfrak{6}_y)\cos 2(\alpha + 90^\circ) \quad (3)$$

where $\varepsilon_{1,2,3}$ = measured strain released from strain gauge, A,B = calibration coefficients, $\mathfrak{6}_x$ = stress in x-direction, and $\mathfrak{6}_y$ = stress in y-direction [27].

Niku-Lari et al. [28] demonstrated the application of finite element analysis in determining correlation coefficients. This method measures strains from the incremental hole-drilling process and uses Mohr circle calculations to obtain the residual stress.

$$\mathfrak{6}_{max} = \frac{\varepsilon_n^1(A_n + B_n \sin 2\theta_n) - \varepsilon_n^2(A_n - B_n \cos 2\theta_n)}{2A_nB_n(\sin 2\theta_n + \cos 2\theta_n)\Delta h_n} \quad (4)$$

$$\mathfrak{6}_{min} = \frac{\varepsilon_n^2(A_n + B_n \cos 2\theta_n) - \varepsilon_n^1(A_n - B_n \sin 2\theta_n)}{2A_nB_n(\sin 2\theta_n + \cos 2\theta_n)\Delta h_n} \quad (5)$$

$$\theta_n = \frac{1}{2} tan^{-1}\left[\frac{\varepsilon_n^1 - 2\varepsilon_n^2 + \varepsilon_n^3}{\varepsilon_n^1 - \varepsilon_n^3}\right] \quad (6)$$

A and B are the calibration coefficients obtained from simulation with ABAQUS software [27], where ε_n^1 and ε_n^3 are the strains at directions 1 and 2 as shown in Fig. 8. Then, Δh_n is the incremental length for each 0.05 mm depth. Also, σ_{1n} and σ_{2n} are the applied pressure set to +30 MPa for A_n and ±30 MPa for B_n.

$$A_n = \frac{\varepsilon_n^1 + \varepsilon_n^3}{2\Delta h_n(\sigma_{1n} + \sigma_{2n})} \quad (7a)$$

$$B_n = \frac{\varepsilon_n^1 - \varepsilon_n^3}{2\Delta h_n(\sigma_{1n} - \sigma_{2n})cos2\theta_n} \quad (7b)$$

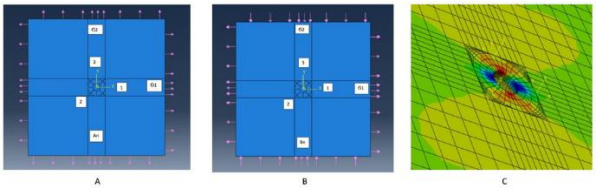

Fig. 8. Determining the loads and directions in FE simulation. A: A_n calibration coefficients, B: B_n calibration coefficients, C: Local coordinate system

The residual stress measurement steps for five specimens were calculated and are given in

the tables from 2 to 6. Then, residual stress directions are displayed on Figs. 9 and 10. The residual stresses are shown as step charts for all specimens from Figs. 11 to 20 based on Mohr's circle.

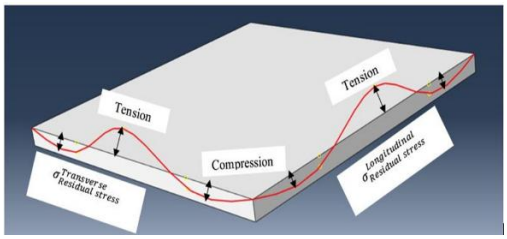

Fig. 9. Display of residual stress directions

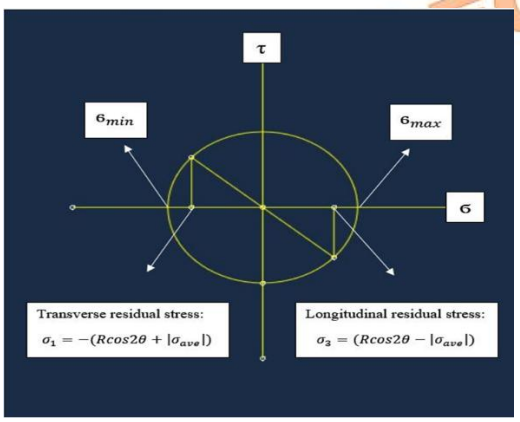

Fig. 10. Stress directions on Mohr's circle

Figure 11 illustrates the transverse residual stress for the Al-Cu specimen. The residual stress on the aluminum side remains relatively constant, dropping from 0 to -2.5 MPa at a depth of 0.15 mm. It then increases to a peak of 33 MPa and continues as tensile residual stress until a depth of 0.35 mm. At this point, the stress becomes compressive, reaching a maximum of -189 MPa at the end of the aluminum layer. Next, the residual stress reaches 78.5 MPa at the beginning of the copper layer, which shows a rise of almost 270 MPa from a depth of 0.5 mm to 0.55 mm. Subsequently, the residual stress falls continuously up to -282 MPa at a depth of 0.7 mm. Then, it grows rapidly to 92.6 MPa at a depth of 0.75 mm. Next, followed by a fall up to -164 MPa at a depth of 0.95 mm. Finally, it reaches a peak of 87 MPa at a depth of 1 mm. Afterward, Fig. 12 shows the longitudinal residual stress for the Al-Cu specimen which is the same as transverse residual stress, but in the opposite directions.

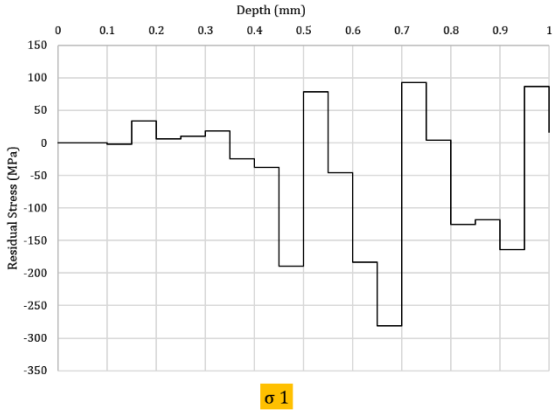

Fig. 11. Transverse residual stress for Al-Cu specimen at Mohr circle

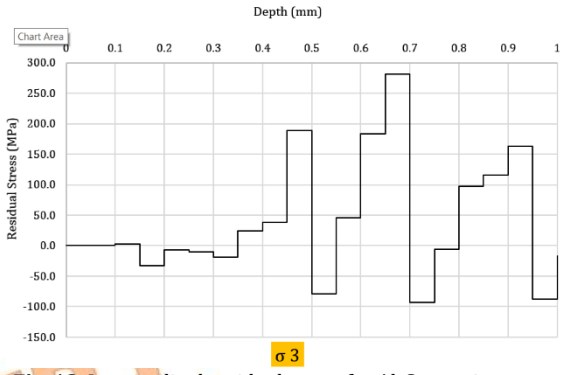

Fig. 12. Longitudinal residual stress for Al-Cu specimen at Mohr circle

Figure 13 depicts the transverse residual stress for the Al-Al specimen. For the top side of the specimen, the tensile residual stress was raised to 110 MPa at a depth of 0.1 mm. Then, the compressive residual stress formed up to -34.6 MPa to the depth of 0.15 mm. Afterward, there is a partial increase in residual stress, reaching up to 13.5 MPa at a depth of 0.2 mm. From this stage onwards, the step curve of the residual stress decreases in an oscillatory manner. Next, the residual stress falls to -36.6 MPa at a depth of 0.35 mm and drops to -120 MPa at a depth of 0.45 mm. Subsequently, the residual stress fluctuates between -42 MPa and -75 MPa at a depth of 0.5 to 0.75 mm. Then, it reaches a peak of -194 MPa at a depth of 0.8mm. Finally, it gradually increases up to -63 MPa at a depth of 1 mm. Next, Fig. 14 presents the longitudinal residual stress for the Al-Al sample, which is similar to the transverse residual stress but acts in the opposite direction.

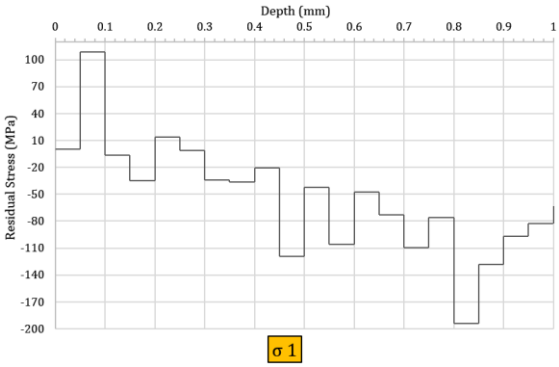

Fig. 13. Transverse residual stress for Al-Al specimen at Mohr circle

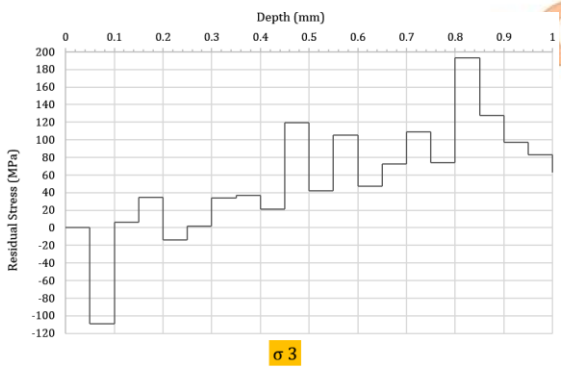

Fig. 14. Longitudinal residual stress for Al-Al specimen at Mohr circle

Figure 15 presents the transverse residual stress for the Cu-Cu specimen. The top half of the specimen has a lower stored residual stress than the bottom half. The top side fluctuates compressively from -11 MPa to tensional 51.4 MPa at a depth of 0.3 mm. Then, it increases rapidly to 270 MPa at a depth of 0.35 mm. Afterward, it drops sharply to 61.5 MPa and reaches a low of -610 MPa at a depth of 0.6 mm. Next, the residual stress peaks at 384 MPa at a depth of 0.65 mm. Subsequently, the residual stress drops to -125 MPa at a depth of 0.8 mm. Then, it climbs to 118 and 135 MPa at a distance of 0.85 and 0.9 mm. Finally, it declines to 117 and 34 MPa at the distance of 0.95 and 1 mm. The compressive and tensile residual stresses fluctuate between ±135 MPa from the beginning to the end of this period. Figure 16 shows the longitudinal residual stress for the Cu-Cu specimen, which represents both equal and opposite directions in transverse residual stress.

Table 2. Residual stress measurement for Al-Cu specimen.

Material	Depth (mm)	ε_1	ε_2	ε_3	A_n (mm/N)	B_n (mm/N)	θ_n	σ_{max} (MPa)	σ_{min} (MPa)	σ_1 (MPa)	σ_3 (MPa)
Al	0.05	4.9E-05	4.9E-05	5.4E-05	-1.1E-08	-1.9E-12	-2.2E+01	4.3E+05	-5.2E+05	-5.2E+05	4.2E+05
	0.1	4.7E-05	4.8E-05	5.6E-05	-7.9E-09	-1.5E-12	-2.0E+01	-3.3E+06	3.2E+06	-2.5E+06	2.4E+06
	0.15	4.8E-05	5.5E-05	5.8E-05	-1.5E-08	-3.5E-12	1.0E+01	6.4E+07	-6.4E+07	3.3E+07	-3.3E+07
	0.2	8.2E-05	8.3E-05	8.8E-05	-1.2E-08	-1.9E-12	-1.2E+01	1.8E+07	-1.9E+07	6.5E+06	-6.6E+06
	0.25	7.6E-05	7.7E-05	1.0E-04	-9.9E-09	-2.0E-12	-2.1E+01	1.9E+07	-1.9E+07	1.0E+07	-1.0E+07
	0.3	8.3E-05	9.2E-05	1.3E-04	-1.3E-08	-3.0E-12	-1.6E+01	-5.1E+07	5.1E+07	1.9E+07	-1.9E+07
	0.35	1.0E-05	1.2E-04	1.7E-04	-1.1E-08	-2.5E-12	-1.2E+01	5.8E+07	-5.8E+07	-2.5E+07	2.4E+07
	0.4	8.8E-05	1.1E-04	1.7E-04	-9.3E-09	-2.6E-12	-1.4E+01	-5.3E+07	5.2E+07	-3.8E+07	3.8E+07
	0.45	4.1E-05	8.9E-05	1.4E-04	-8.3E-09	-2.3E-12	-1.5E+00	-1.9E+08	1.9E+08	-1.9E+08	1.9E+08
	0.5	4.9E-05	9.9E-05	1.5E-04	-5.7E-09	3.2E-12	-1.2E+00	1.1E+08	-1.1E+08	7.8E+07	-7.9E+07
Cu	0.55	8.2E-05	1.3E-04	2.0E-04	-1.2E-08	-3.4E-12	-2.6E+00	1.2E+08	-1.2E+08	-4.6E+07	4.6E+07
	0.6	9.1E-05	1.4E-04	2.1E-04	-1.1E-08	-4.1E-12	-3.3E+00	1.9E+08	-1.9E+08	-1.8E+08	1.8E+08
	0.65	9.1E-05	1.5E-04	2.2E-04	-5.4E-09	-2.7E-12	-3.3E+00	2.9E+08	-2.9E+08	-2.8E+08	2.8E+08
	0.7	1.1E-04	1.8E-04	2.5E-04	-4.5E-09	-3.3E-12	-2.2E+00	3.0E+08	-3.0E+08	9.3E+07	-9.3E+07
	0.75	1.8E-04	2.4E-04	3.2E-04	-2.1E-09	-3.1E-12	-3.9E+00	-2.1E+08	2.0E+08	4.5E+06	-6.2E+06
	0.8	2.4E-04	3.0E-04	3.9E-04	2.0E-10	-2.9E-12	-6.0E+00	1.5E+08	-1.2E+08	-1.2E+08	9.7E+07
	0.85	2.2E-04	2.7E-04	3.6E-04	2.5E-09	-2.8E-12	-6.0E+00	1.5E+08	-1.5E+08	-1.2E+08	1.2E+08
	0.9	2.3E-04	2.9E-04	3.7E-04	4.9E-09	-2.7E-12	-6.1E+00	1.7E+08	-1.7E+08	-1.6E+08	1.6E+08
	0.95	2.4E-04	2.9E-04	3.9E-04	8.3E-09	-2.9E-12	-6.9E+00	-2.9E+08	2.9E+08	8.7E+07	-8.7E+07
	1	2.3E-04	2.9E-04	3.8E-04	1.6E-08	-3.8E-12	-7.0E+00	-1.7E+08	1.7E+08	1.7E+07	-1.7E+07

Table 3. Residual stress measurement for Al-Al specimen.

Material	Depth (mm)	ε_1	ε_2	ε_3	A_n (mm/N)	B_n (mm/N)	θ_n	σ_{max} (MPa)	σ_{min} (MPa)	σ_1 (MPa)	σ_3 (MPa)
Al	0.05	2.1E-06	5.1E-06	-5.7E-06	-1.2E-08	-2.6E-12	-3.0E+01	1.6E+08	-1.6E+08	1.1E+08	-1.1E+08
	0.1	1.0E-05	1.2E-05	3.8E-06	-8.5E-09	-1.8E-12	-2.8E+01	7.0E+06	-7.0E+06	-6.6E+06	6.5E+06
	0.15	1.9E-05	2.3E-05	1.2E-05	-1.5E-08	-3.3E-12	-3.2E+01	4.2E+07	-4.2E+07	-3.5E+07	3.5E+07
	0.2	2.8E-05	9.9E-06	1.7E-05	-1.3E-08	-2.2E-12	3.4E+01	7.0E+07	-7.0E+07	1.3E+07	-1.3E+07
	0.25	1.7E-05	1.8E-05	1.0E-05	-1.1E-08	-2.5E-12	-2.5E+01	1.8E+06	-1.8E+06	-1.6E+06	1.6E+06
	0.3	1.5E-05	2.6E-05	-3.4E-06	-1.4E-08	-3.3E-12	-3.3E+01	-3.4E+07	3.4E+07	-3.4E+07	3.4E+07
	0.35	2.1E-05	4.0E-05	-2.7E-06	-1.2E-08	-3.1E-12	-3.4E+01	4.3E+07	-4.3E+07	-3.7E+07	3.7E+07
	0.4	2.0E-05	4.3E-05	-3.7E-06	-1.1E-08	-3.2E-12	-3.6E+01	-5.5E+07	5.5E+07	-2.1E+07	2.1E+07
	0.45	2.8E-05	5.6E-05	-5.8E-06	-9.8E-09	-3.2E-12	-3.5E+01	1.2E+08	-1.2E+08	-1.2E+08	1.2E+08
	0.5	2.1E-05	5.5E-05	-1.3E-05	-1.1E-08	-4.4E-12	-3.6E+01	-5.5E+07	5.5E+07	-4.2E+07	4.2E+07
Al	0.55	3.1E-05	5.9E-05	-2.8E-06	-9.1E-09	-4.2E-12	-3.5E+01	1.1E+08	-1.1E+08	-1.1E+08	1.1E+08
	0.6	3.3E-05	5.2E-05	-1.9E-05	-8.2E-09	-4.6E-12	-3.0E+01	-4.8E+07	4.8E+07	-4.7E+07	4.7E+07
	0.65	3.1E-05	6.1E-05	-1.9E-05	-3.8E-09	-3.0E-12	-3.3E+01	-7.7E+07	7.7E+07	-7.3E+07	7.2E+07
	0.7	1.3E-05	6.1E-05	-3.3E-05	-2.8E-09	-3.7E-12	-3.6E+01	-1.1E+08	1.1E+08	-1.1E+08	1.1E+08
	0.75	2.0E-05	6.9E-05	-2.9E-05	-6.6E-10	-3.6E-12	-3.6E+01	-9.8E+07	9.6E+07	-7.6E+07	7.4E+07
	0.8	-6.0E-06	6.2E-05	-5.4E-05	1.6E-09	-3.5E-12	-3.8E+01	1.9E+08	-1.9E+08	-1.9E+08	1.9E+08
	0.85	-8.1E-06	5.6E-05	-4.2E-05	4.2E-09	-3.4E-12	-3.9E+01	-1.4E+08	1.4E+08	-1.3E+08	1.3E+08
	0.9	5.2E-06	6.7E-05	-5.7E-05	7.4E-09	-3.5E-12	-3.6E+01	-1.3E+08	1.3E+08	-9.7E+07	9.7E+07
	0.95	9.0E-06	6.8E-05	-5.0E-05	1.2E-08	-3.9E-12	-3.6E+01	-1.1E+08	1.1E+08	-8.3E+07	8.3E+07
	1	1.1E-05	6.8E-05	-4.5E-05	2.3E-08	-4.9E-12	-3.6E+01	-8.1E+07	8.2E+07	-6.3E+07	6.3E+07

Table 4. Residual stress measurement for Cu-Cu specimen.

Material	Depth (mm)	ε_1	ε_2	ε_3	A_n (mm/N)	B_n (mm/N)	θ_n	σ_{max} (MPa)	σ_{min} (MPa)	σ_1 (MPa)	σ_3 (MPa)
Cu	0.05	-9.0E-07	-1.8E-06	-5.0E-07	-6.9E-09	-1.6E-12	-4.0E+01	-1.1E+07	1.1E+07	-4.4E+06	4.4E+06
	0.1	-9.0E-07	-3.8E-06	-3.0E-07	-5.0E-09	-1.1E-12	-4.2E+01	2.3E+07	-2.3E+07	2.3E+07	-2.3E+07
	0.15	-5.0E-07	-5.9E-06	-1.6E-06	-9.0E-09	-2.0E-12	4.2E+01	-4.0E+07	4.0E+07	-1.1E+07	1.1E+07
	0.2	6.0E-07	-6.5E-06	-1.1E-06	-8.0E-09	-1.3E-12	4.1E+01	-3.8E+07	3.8E+07	3.2E+07	-3.2E+07
	0.25	3.2E-06	-6.1E-06	1.2E-06	-7.0E-09	-1.5E-12	4.2E+01	-5.6E+07	5.6E+07	6.7E+06	-6.7E+06
	0.3	5.7E-06	-6.0E-06	3.8E-06	-8.4E-09	-2.0E-12	4.2E+01	5.2E+07	-5.2E+07	5.1E+07	-5.1E+07
	0.35	1.0E-05	-5.2E-06	3.5E-06	-7.5E-09	-1.9E-12	3.7E+01	-3.3E+08	3.3E+08	2.7E+08	-2.7E+08
	0.4	1.1E-05	-5.7E-06	2.1E-06	-6.8E-09	-1.9E-12	3.5E+01	-6.7E+07	6.7E+07	6.2E+07	-6.2E+07
	0.45	1.4E-05	-4.5E-06	4.1E-06	-6.2E-09	-1.9E-12	3.5E+01	-6.9E+07	6.9E+07	5.8E+07	-5.8E+07
	0.5	1.7E-05	-2.8E-06	6.4E-06	-7.0E-09	-2.7E-12	3.5E+01	-5.4E+07	5.4E+07	4.5E+07	-4.5E+07
Cu	0.55	2.1E-05	2.0E-07	7.8E-06	-5.8E-09	-2.5E-12	3.2E+01	-2.0E+08	2.0E+08	-9.7E+07	9.7E+07
	0.6	2.0E-05	-3.4E-06	5.1E-06	-5.2E-09	-2.8E-12	3.3E+01	-9.2E+08	9.2E+08	-6.1E+08	6.1E+08
	0.65	2.4E-05	9.0E-07	1.1E-05	-2.4E-09	-1.8E-12	3.4E+01	-4.6E+08	4.6E+08	3.8E+08	-3.8E+08
	0.7	2.9E-05	4.5E-06	1.8E-05	-1.9E-09	-2.2E-12	3.7E+01	8.8E+07	-8.8E+07	2.6E+07	-2.6E+07
	0.75	3.6E-05	1.3E-05	2.1E-05	-5.5E-10	-2.1E-12	3.2E+01	-8.1E+07	8.0E+07	6.9E+07	-7.0E+07
	0.8	3.9E-05	1.2E-05	2.3E-05	8.6E-10	-2.1E-12	3.4E+01	2.8E+08	-2.8E+08	-1.2E+08	1.2E+08

	0.85	4.5E-05	2.0E-05	2.8E-05	2.4E-09	-2.0E-12	3.1E+01	-1.2E+08	1.2E+08	1.2E+08	-1.2E+08
	0.9	4.8E-05	1.8E-05	2.7E-05	4.4E-09	-2.0E-12	3.1E+01	-1.4E+08	1.4E+08	1.4E+08	-1.4E+08
	0.95	4.9E-05	1.6E-05	2.7E-05	7.4E-09	-2.3E-12	3.2E+01	-1.2E+08	1.2E+08	1.2E+08	-1.2E+08
	1	3.0E-05	3.3E-06	4.8E-06	1.4E-08	-2.8E-12	2.4E+01	7.1E+07	-7.1E+07	3.4E+07	-3.4E+07

Table 5. Transverse tensile residual stress for all specimens using Mohr's circle method

	First layer		Second layer		Third layer	
	Minimum (MPa)	Maximum (MPa)	Minimum (MPa)	Maximum (MPa)	Minimum (MPa)	Maximum (MPa)
Al-Al	13.5	108.8	0	0	—	—
Cu-Cu	22.7	269.4	69	384	—	—
Al-Cu	6.5	33.1	78.4	92.6	—	—
Al-Cu-Al	17	53	14	16	61.7	133
Cu-Al-Cu	8	19	13	68	5.4	313.8

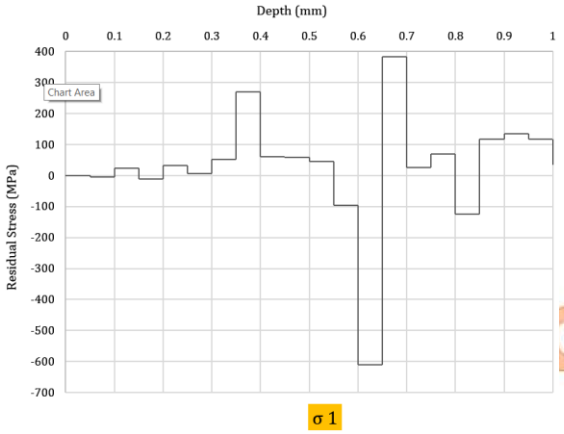

Fig. 15. Transverse residual stress for Cu-Cu specimen at Mohr circle

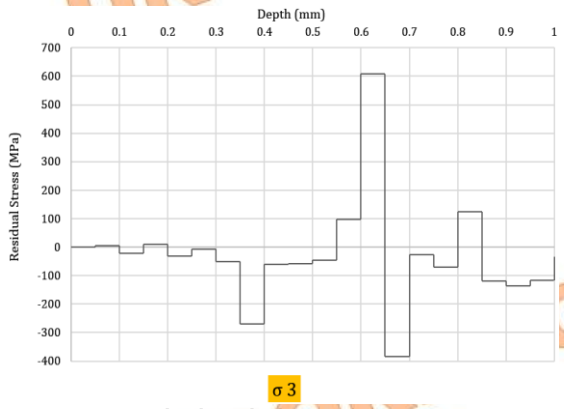

Fig. 16. Longitudinal residual stress for Cu-Cu specimen at Mohr circle

Figure 17 shows the transverse residual stress for the Al-Cu-Al specimen. In this three-layer sample, the range of residual stress fluctuation is approximately between -89 MPa and 133 MPa. The lowest step of the compressive residual stress for the top aluminum side is -64 MPa at the depth of 0.05 mm, and the highest step of the tensile residual stress for the same layer is 53.4 MPa at the depth of 0.2 mm. The lower bound of the compressive residual stress for the middle layer, copper, is -88.7 MPa at a depth of 0.55 mm, and the upper bound of the tensile residual stress for the similar layer is 16 MPa at a depth of 0.6 mm. Subsequently, the residual goes up to 133 MPa at a depth of 0.75 mm. Then, it falls to 70 MPa at a depth of 0.8 mm. Next, followed by a growth up to 61.7 MPa at the depth of 0.85 mm. Finally, it decreases gradually from -96.7 MPa at a depth of 0.9 mm to -575 MPa at a depth of 1 mm. Figure 18 shows the longitudinal residual stress for the Al-Cu-Al specimen which is the same as the transverse one, however, in the opposite direction.

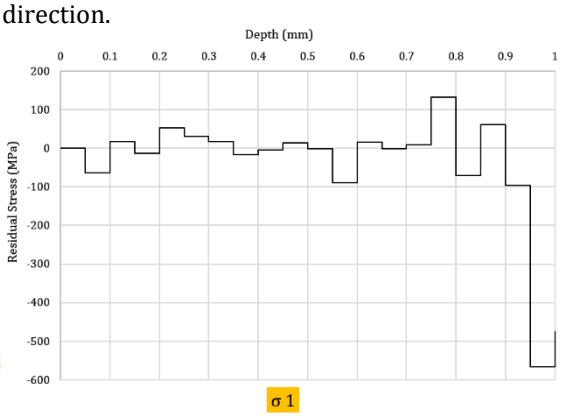

Fig. 17. Transverse residual stress for Al-Cu-Al specimen at Mohr circle

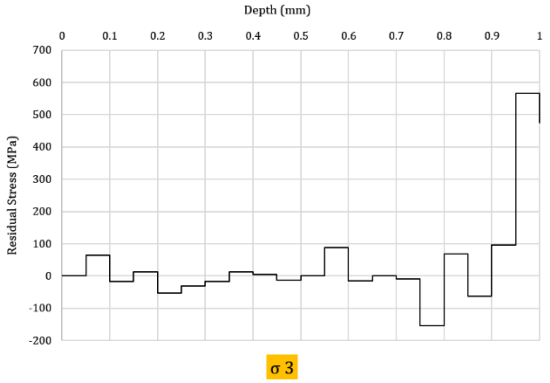

Fig. 18. Longitudinal residual stress for Al-Cu-Al specimen at Mohr circle

Figure 19 exhibits the residual stress for the Cu-Al-Cu specimen at transverse directions. The residual stress fluctuates between -56.2 MPa and 68.6 MPa. The first layer typically exhibits compressive residual stress, while the middle and bottom layers tend to have tensile residual stress. Then, it reaches a peak of 314 MPa at a depth of 0.9 mm. Following, Fig. 20 indicates the longitudinal residual stress for the Cu-Al-Cu specimen which is relevant to transverse residual stress, even so in opposite directions.

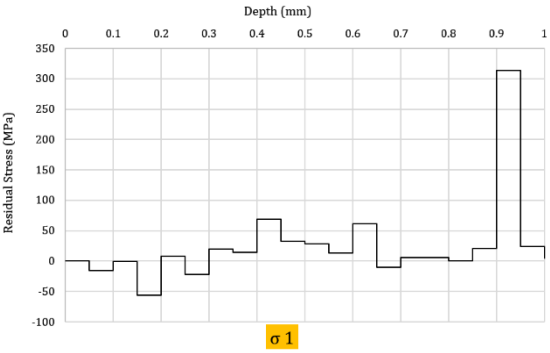

Fig. 19. Transverse residual stress for Cu-Al-Cu specimen at Mohr circle

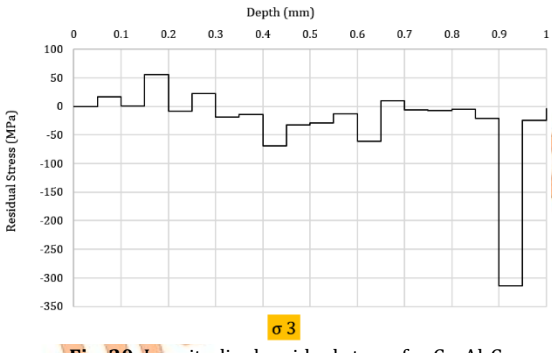

Fig. 20. Longitudinal residual stress for Cu-Al-Cu specimen at Mohr circle

According to this study, five experiments employing aluminum and copper metals with different layups of fabricated composite specimens were conducted using the CRB process. The resulting strains of the incremental hole drilling were measured using rosette strain gauges based on the ASTM E837-13a standard. An overview of the obtained results shows that the majority of residual stress fluctuations occur in the copper layer of the Al-Cu sample, which is -282 MPa compressive residual stress in the transverse direction. For the Al-Al specimen, the highest stored residual stress is compressive, -192 MPa, and occurred in the transverse direction of the second layer. The highest amount of stored compressive residual stress can be seen in the bottom layer of the Cu-Cu sample, which is -610 MPa in the transverse direction. Three-layered specimens have less stored residual stress fluctuations compared to two-layered specimens. Likewise, the highest stored compressive residual stress appeared in the last layer of these samples. Al-Cu-Al with -575 MPa and Cu-Al-Cu with -314 MPa are the next observations in transverse and longitudinal directions, respectively.

Additionally, considering the critical role of tensile residual stresses in reducing structural lifespan and increasing the likelihood of crack propagation, the tensile residual stresses in the transverse direction induced in the laminated layers of the roll-bonded samples, addressing their maximum and minimum values at each layer outlined in Table 5. Based on the presented data, the highest tensile residual stress is related to the two-layer samples, where the stress stored in the copper layer exceeds that in the aluminum layer.

4. Conclusion

In this research, an investigation was implemented to determine the effect of residual stress on two and three-layer composite specimens with different sequences of aluminum and copper metals. The CRB process of specimens was prepared by a rolling machine and the residual stress measurement was taken by the incremental hole-drilling strain gauge method. The results were calculated via experimental and finite element methods. The notable outcomes are listed below:

- The ultimate tensile strength of aluminum mono-layer was lower than all composite specimens.
- The ultimate tensile strength of the copper mono-layer was higher than all samples, except rolled Cu-Cu one.
- Residual stress values in two-layer samples are higher than three-layer ones.
- In general, copper metal has stored more residual stress than aluminum metal.
- The layers were located far from the drilling bit and recorded much higher residual stress.
- In transverse direction calculations, from 0.5 mm thickness to 1 mm thickness, the highest

values of residual stress are compressive residual stress.

- Tensile residual stresses decrease the lifespan of structures and promote the growth of cracks. The highest tensile residual stress is related to the two-layer samples, especially the copper layer.

Nomenclature

CRB	Cold Roll Boning
FEA	Finite Element Analysis
ESPI	Electronic Speckle Pattern Interferometry
$\varepsilon_{1,2,3}$	Measured strains released from strain gauge
A, B	Calibration coefficients
$\mathfrak{6}_x$, $\mathfrak{6}_y$	Stresses in x and y direction
$\mathfrak{6}_{max}$	Maximum Stress
$\mathfrak{6}_{min}$	Minimum Stress
ε_n^1, ε_n^3	Strains at directions 1 and 2
σ_{1n}, σ_{2n}	Applied pressure
Δh_n	Incremental length

Funding Statement

This research did not receive any specific grant from funding agencies in the public, commercial, or not-for-profit sectors.

Conflicts of Interest

The author declares that there is no conflict of interest regarding the publication of this article.

References

[1] Schajer G. S., 1988. Measurement of Non-Uniform Residual Stresses Using the Hole-Drilling Method. Part I—Stress Calculation Procedures. Journal of Engineering Materials and Technology, 110(4). pp. 338–343.

[2] Sedighi M., Honarpisheh M., 2012. Investigation of cold rolling influence on near surface residual stress distribution in explosive welded multilayer. Strength Mater, vol. 44, pp. 693-698.

[3] James M. N., Hattingh D. G., Asquith D., Newby M., Doubell P., 2016. Applications of Residual Stress in Combatting Fatigue and Fracture. Procedia Structural Integrity, vol. 2, pp. 11–25.

[4] ASTM E837-20, 2023. Standard Test Method for Determining Residual Stresses by the Hole-Drilling Strain-Gage Method. https://www.astm.org/e0837-13a.html.

[5] Ma Y., Yao X., Zhang D., 2015. Axially symmetrical stress measurement in the cylindrical tube using DIC with hole drilling. Optics and Lasers in Engineering, vol. 66, pp. 174–180.

[6] Chen H., Song Y., Chen X., Yu X., Chen S., 2020. In situ studies of full-field residual stress mapping of SS304 stainless steel welds using DIC. Int J Adv Manuf Technol, vol. 109, no. 1, pp. 45–55.

[7] Babaeeian M., Mohammadimehr M., 2021. Experimental and computational analyses on residual stress of composite plate using DIC and Hole-drilling methods based on Mohr's circle and considering the time effect. Optics and Lasers in Engineering, vol. 137, p. 106355.

[8] Babaeeian M., Mohammadimehr M., 2020. Investigation of the time elapsed effect on residual stress measurement in a composite plate by DIC method. Optics and Lasers in Engineering, vol. 128, p. 106002.

[9] Steinzig M., Upshaw D., Rasty J., 2014. Influence of Drilling Parameters on the Accuracy of Hole-drilling Residual Stress Measurements. Exp Mech, vol. 54, no. 9, pp. 1537–1543.

[10] Blödorn R., Viotti M. R., Schroeter R. B., Albertazzi A., 2015. Analysis of Blind-Holes Applied in the Hole-Drilling Method for Residual Stress Measurements. Exp Mech, vol. 55, no. 9, pp. 1745–1756.

[11] Rickert T., 2016. Residual Stress Measurement by ESPI Hole-Drilling. Procedia CIRP, vol. 45, pp. 203–206.

[12] Bonnet C., Pottier T., Landon Y., 2021. Development of a multi-scale and coupled cutting model for the drilling of Ti-6Al-4V. CIRP Journal of Manufacturing Science and Technology, vol. 35, pp. 526–540.

[13] Shi X., Hussain G., Butt S. I., Song F., Huang D., Liu Y., 2017. The state of residual stresses in the Cu/Steel bonded laminates after ISF deformation: An experimental analysis. Journal of Manufacturing Processes, vol. 30, pp. 14–26.

[14] Sedighi M., Honarpisheh M., 2012. Experimental study of through-depth residual stress in explosive welded Al–Cu–Al multilayer. Mater Des, vol. 37, pp. 577–581.

[15] Alinaghian M., Alinaghian I., Honarpisheh M., 2019. Residual stress measurement of single point incremental formed Al/Cu bimetal using the incremental hole-drilling method. International Journal of Lightweight Materials and Manufacture, vol. 2, no. 2, pp. 131–139.

[16] Tamonov A. V., Sumin V. V., 2004. Investigation of Residual Stresses in a Bimetallic Stainless Steel–Zirconium Adapter by Neutron Diffraction. Journal of Neutron Research, vol. 12, no. 1–3, pp. 69–73.

[17] Varavallo R., Moreira M., Paes V., Brito P., Olivas J., Pinto H. C., 2014. Microstructure and Residual Stress Analysis of Explosion Cladded Inconel 625 and ASME SA516-70 Carbon Steel

Bimetal Plates. Advanced Materials Research, vol. 996, pp. 494–499.

[18] Fronczek D. M., et al., 2018. Residual stress distribution, correlated with bending tests, within explosively welded Ti gr. 2/A1050 bimetals. Materials Characterization, vol. 144, pp. 461–468.

[19] Kotobi M., Honarpisheh M., 2018. Through-depth residual stress measurement of laser-bent steel–titanium bimetal sheets. The Journal of Strain Analysis for Engineering Design, vol. 53, no. 3, pp. 130–140.

[20] Kotobi M., Mansouri H., Honarpisheh M., 2019. Investigation of laser bending parameters on the residual stress and bending angle of St-Ti bimetal using FEM and neural network. Optics & Laser Technology, vol. 116, pp. 265–275.

[21] Dong F., Yi Y., Huang S., 2020. Measuring internal residual stress in Al-Cu alloy forgings by crack compliance method with optimized parameters. J. Cent. South Univ., vol. 27, no. 11, pp. 3163–3174.

[22] Xie W., Tomiko Y., Kazumasa K., 2012. Formation of Intermetallic Compounds on the Bond Interface of Aluminum-Clad Copper and its Influence on Bond Tensile Strength. Applied Mechanics and Materials, vol. 117–119, pp. 984–989.

[23] Mao Z., Xie J., Wang A., Wang W., Ma D., Liu P., 2020. Effects of annealing temperature on the interfacial microstructure and bonding strength of Cu/Al clad sheets produced by twin-roll casting and rolling. Journal of Materials Processing Technology, vol. 285, p. 116804.

[24] Biyik S., 2018. Effect of Reinforcement Ratio on Physical and Mechanical Properties of Cu-W Composites Synthesized by Ball Milling. Materials Focus, vol. 7, no. 4, pp. 535–541.

[25] Jamaati R., Toroghinejad M. R., 2011. Cold roll bonding bond strengths. Materials Science and Technology, vol. 27, no. 7, pp. 1101–1108.

[26] ASTM E8/E8M-22., 2024. Standard Test Methods for Tension Testing of Metallic Materials. https://store.astm.org/e0008_e0008m-22.html.

[27] ASTM E837-20., 2021. Standard Test Method for Determining Residual Stresses by the Hole-Drilling Strain-Gage Method. https://store.astm.org/e0837-20.html.

[28] Niku-Lari A., Lu J., Flavenot F., 1985. Measurement of residual-stress distribution by the incremental hole-drilling method. Journal of Mechanical Working Technology, vol. 11, no. 2, pp. 167–188.